

Search for pair production of the scalar top quark in muon+tau final states

V.M. Abazov,³⁴ B. Abbott,⁷² B.S. Acharya,²⁸ M. Adams,⁴⁸ T. Adams,⁴⁶ G.D. Alexeev,³⁴ G. Alkhazov,³⁸ A. Alton^a,⁶⁰ G. Alverson,⁵⁹ M. Aoki,⁴⁷ A. Askew,⁴⁶ B. Åsman,⁴⁰ S. Atkins,⁵⁷ O. Atramentov,⁶⁴ K. Augsten,⁹ C. Avila,⁷ J. BackusMayes,⁷⁹ F. Badaud,¹² L. Bagby,⁴⁷ B. Baldin,⁴⁷ D.V. Bandurin,⁴⁶ S. Banerjee,²⁸ E. Barberis,⁵⁹ P. Baringer,⁵⁵ J. Barreto,³ J.F. Bartlett,⁴⁷ U. Bassler,¹⁷ V. Bazterra,⁴⁸ A. Bean,⁵⁵ M. Begalli,³ C. Belanger-Champagne,⁴⁰ L. Bellantoni,⁴⁷ S.B. Beri,²⁶ G. Bernardi,¹⁶ R. Bernhard,²¹ I. Bertram,⁴¹ M. Besançon,¹⁷ R. Beuselinck,⁴² V.A. Bezzubov,³⁷ P.C. Bhat,⁴⁷ S. Bhatia,⁶² V. Bhatnagar,²⁶ G. Blazey,⁴⁹ S. Blessing,⁴⁶ K. Bloom,⁶³ A. Boehnlein,⁴⁷ D. Boline,⁶⁹ E.E. Boos,³⁶ G. Borissov,⁴¹ T. Bose,⁵⁸ A. Brandt,⁷⁵ O. Brandt,²² R. Brock,⁶¹ G. Brooijmans,⁶⁷ A. Bross,⁴⁷ D. Brown,¹⁶ J. Brown,¹⁶ X.B. Bu,⁴⁷ M. Buehler,⁴⁷ V. Buescher,²³ V. Bunichev,³⁶ S. Burdin,⁴¹ T.H. Burnett,⁷⁹ C.P. Buszello,⁴⁰ B. Calpas,¹⁴ E. Camacho-Pérez,³¹ M.A. Carrasco-Lizarraga,⁵⁵ B.C.K. Casey,⁴⁷ H. Castilla-Valdez,³¹ S. Chakrabarti,⁶⁹ D. Chakraborty,⁴⁹ K.M. Chan,⁵³ A. Chandra,⁷⁷ E. Chapon,¹⁷ G. Chen,⁵⁵ S. Chevalier-Théry,¹⁷ D.K. Cho,⁷⁴ S.W. Cho,³⁰ S. Choi,³⁰ B. Choudhary,²⁷ S. Cihangir,⁴⁷ D. Claes,⁶³ J. Clutter,⁵⁵ M. Cooke,⁴⁷ W.E. Cooper,⁴⁷ M. Corcoran,⁷⁷ F. Couderc,¹⁷ M.-C. Cousinou,¹⁴ A. Croc,¹⁷ D. Cutts,⁷⁴ A. Das,⁴⁴ G. Davies,⁴² S.J. de Jong,³³ E. De La Cruz-Burelo,³¹ F. Déliot,¹⁷ R. Demina,⁶⁸ D. Denisov,⁴⁷ S.P. Denisov,³⁷ S. Desai,⁴⁷ C. Deterre,¹⁷ K. DeVaughan,⁶³ H.T. Diehl,⁴⁷ M. Diesburg,⁴⁷ P.F. Ding,⁴³ A. Dominguez,⁶³ T. Dorland,⁷⁹ A. Dubey,²⁷ L.V. Dudko,³⁶ D. Duggan,⁶⁴ A. Duperrin,¹⁴ S. Dutt,²⁶ A. Dyshkant,⁴⁹ M. Eads,⁶³ D. Edmunds,⁶¹ J. Ellison,⁴⁵ V.D. Elvira,⁴⁷ Y. Enari,¹⁶ H. Evans,⁵¹ A. Evdokimov,⁷⁰ V.N. Evdokimov,³⁷ G. Facini,⁵⁹ T. Ferbel,⁶⁸ F. Fiedler,²³ F. Filthaut,³³ W. Fisher,⁶¹ H.E. Fisk,⁴⁷ M. Fortner,⁴⁹ H. Fox,⁴¹ S. Fuess,⁴⁷ A. Garcia-Bellido,⁶⁸ G.A. García-Guerra^c,³¹ V. Gavrilov,³⁵ P. Gay,¹² W. Geng,^{14,61} D. Gerbaudo,⁶⁵ C.E. Gerber,⁴⁸ Y. Gershtein,⁶⁴ G. Ginther,^{47,68} G. Golovanov,³⁴ A. Goussiou,⁷⁹ P.D. Grannis,⁶⁹ S. Greder,¹⁸ H. Greenlee,⁴⁷ Z.D. Greenwood,⁵⁷ E.M. Gregores,⁴ G. Grenier,¹⁹ Ph. Gris,¹² J.-F. Grivaz,¹⁵ A. Grohsjeanⁱ,¹⁷ S. Grünendahl,⁴⁷ M.W. Grünewald,²⁹ T. Guillemin,¹⁵ G. Gutierrez,⁴⁷ P. Gutierrez,⁷² A. Haas^d,⁶⁷ S. Hagopian,⁴⁶ J. Haley,⁵⁹ L. Han,⁶ K. Harder,⁴³ A. Harel,⁶⁸ J.M. Hauptman,⁵⁴ J. Hays,⁴² T. Head,⁴³ T. Hebbeker,²⁰ D. Hedin,⁴⁹ H. Hegab,⁷³ A.P. Heinson,⁴⁵ U. Heintz,⁷⁴ C. Hensel,²² I. Heredia-De La Cruz,³¹ K. Herner,⁶⁰ G. Hesketh^e,⁴³ M.D. Hildreth,⁵³ R. Hirosky,⁷⁸ T. Hoang,⁴⁶ J.D. Hobbs,⁶⁹ B. Hoeneisen,¹¹ M. Hohlfeld,²³ Z. Hubacek,^{9,17} V. Hynek,⁹ I. Iashvili,⁶⁶ Y. Ilchenko,⁷⁶ R. Illingworth,⁴⁷ A.S. Ito,⁴⁷ S. Jabeen,⁷⁴ M. Jaffré,¹⁵ D. Jamin,¹⁴ A. Jayasinghe,⁷² R. Jesik,⁴² K. Johns,⁴⁴ M. Johnson,⁴⁷ A. Jonckheere,⁴⁷ P. Jonsson,⁴² J. Joshi,²⁶ A.W. Jung,⁴⁷ A. Juste,³⁹ K. Kaadze,⁵⁶ E. Kajfasz,¹⁴ D. Karmanov,³⁶ P.A. Kasper,⁴⁷ I. Katsanos,⁶³ R. Kehoe,⁷⁶ S. Kermiche,¹⁴ N. Khalatyan,⁴⁷ A. Khanov,⁷³ A. Kharchilava,⁶⁶ Y.N. Kharzheev,³⁴ J.M. Kohli,²⁶ A.V. Kozelov,³⁷ J. Kraus,⁶¹ S. Kulikov,³⁷ A. Kumar,⁶⁶ A. Kupco,¹⁰ T. Kurča,¹⁹ V.A. Kuzmin,³⁶ S. Lammers,⁵¹ G. Landsberg,⁷⁴ P. Lebrun,¹⁹ H.S. Lee,³⁰ S.W. Lee,⁵⁴ W.M. Lee,⁴⁷ J. Lellouch,¹⁶ H. Li,¹³ L. Li,⁴⁵ Q.Z. Li,⁴⁷ S.M. Lietti,⁵ J.K. Lim,³⁰ D. Lincoln,⁴⁷ J. Linnemann,⁶¹ V.V. Lipaev,³⁷ R. Lipton,⁴⁷ Y. Liu,⁶ A. Lobodenko,³⁸ M. Lokajicek,¹⁰ R. Lopes de Sa,⁶⁹ H.J. Lubatti,⁷⁹ R. Luna-Garcia^f,³¹ A.L. Lyon,⁴⁷ A.K.A. Maciel,² D. Mackin,⁷⁷ R. Madar,¹⁷ R. Magaña-Villalba,³¹ S. Malik,⁶³ V.L. Malyshev,³⁴ Y. Maravin,⁵⁶ J. Martínez-Ortega,³¹ R. McCarthy,⁶⁹ C.L. McGivern,⁵⁵ M.M. Meijer,³³ A. Melnitchouk,⁶² D. Menezes,⁴⁹ P.G. Mercadante,⁴ M. Merkin,³⁶ A. Meyer,²⁰ J. Meyer,²² F. Miconi,¹⁸ N.K. Mondal,²⁸ G.S. Muanza,¹⁴ M. Mulhearn,⁷⁸ E. Nagy,¹⁴ M. Naimuddin,²⁷ M. Narain,⁷⁴ R. Nayyar,²⁷ H.A. Neal,⁶⁰ J.P. Negret,⁷ P. Neustroev,³⁸ S.F. Novaes,⁵ T. Nunnemann,²⁴ G. Obrant[†],³⁸ J. Orduna,⁷⁷ N. Osman,¹⁴ J. Osta,⁵³ G.J. Otero y Garzón,¹ M. Padilla,⁴⁵ A. Pal,⁷⁵ N. Parashar,⁵² V. Parihar,⁷⁴ S.K. Park,³⁰ R. Partridge^d,⁷⁴ N. Parua,⁵¹ A. Patwa,⁷⁰ B. Penning,⁴⁷ M. Perfilov,³⁶ Y. Peters,⁴³ K. Petridis,⁴³ G. Petrillo,⁶⁸ P. Pétroff,¹⁵ R. Piegai,¹ M.-A. Pleier,⁷⁰ P.L.M. Podesta-Lerma^g,³¹ V.M. Podstavkov,⁴⁷ P. Polozov,³⁵ A.V. Popov,³⁷ M. Prewitt,⁷⁷ D. Price,⁵¹ N. Prokopenko,³⁷ J. Qian,⁶⁰ A. Quadt,²² B. Quinn,⁶² M.S. Rangel,² K. Ranjan,²⁷ P.N. Ratoff,⁴¹ I. Razumov,³⁷ P. Renkel,⁷⁶ M. Rijssenbeek,⁶⁹ I. Ripp-Baudot,¹⁸ F. Rizatdinova,⁷³ M. Rominsky,⁴⁷ A. Ross,⁴¹ C. Royon,¹⁷ P. Rubinov,⁴⁷ R. Ruchti,⁵³ G. Safronov,³⁵ G. Sajot,¹³ P. Salcido,⁴⁹ A. Sánchez-Hernández,³¹ M.P. Sanders,²⁴ B. Sanghi,⁴⁷ A.S. Santos,⁵ G. Savage,⁴⁷ L. Sawyer,⁵⁷ T. Scanlon,⁴² R.D. Schamberger,⁶⁹ Y. Scheglov,³⁸ H. Schellman,⁵⁰ T. Schliephake,²⁵ S. Schlobohm,⁷⁹ C. Schwanenberger,⁴³ R. Schwienhorst,⁶¹ J. Sekaric,⁵⁵ H. Severini,⁷² E. Shabalina,²² V. Shary,¹⁷ A.A. Shchukin,³⁷ R.K. Shivpuri,²⁷ V. Simak,⁹ V. Sirotenko,⁴⁷ P. Skubic,⁷² P. Slattery,⁶⁸ D. Smirnov,⁵³ K.J. Smith,⁶⁶ G.R. Snow,⁶³ J. Snow,⁷¹

S. Snyder,⁷⁰ S. Söldner-Rembold,⁴³ L. Sonnenschein,²⁰ K. Soustruznik,⁸ J. Stark,¹³ V. Stolin,³⁵ D.A. Stoyanova,³⁷ M. Strauss,⁷² D. Strom,⁴⁸ L. Stutte,⁴⁷ L. Suter,⁴³ P. Svoisky,⁷² M. Takahashi,⁴³ A. Tanasijczuk,¹ M. Titov,¹⁷ V.V. Tokmenin,³⁴ Y.-T. Tsai,⁶⁸ K. Tschann-Grimm,⁶⁹ D. Tsybychev,⁶⁹ B. Tuchming,¹⁷ C. Tully,⁶⁵ L. Uvarov,³⁸ S. Uvarov,³⁸ S. Uzunyan,⁴⁹ R. Van Kooten,⁵¹ W.M. van Leeuwen,³² N. Varelas,⁴⁸ E.W. Varnes,⁴⁴ I.A. Vasilyev,³⁷ P. Verdier,¹⁹ L.S. Vertogradov,³⁴ M. Verzocchi,⁴⁷ M. Vesterinen,⁴³ D. Vilanova,¹⁷ P. Vokac,⁹ H.D. Wahl,⁴⁶ M.H.L.S. Wang,⁴⁷ J. Warchol,⁵³ G. Watts,⁷⁹ M. Wayne,⁵³ M. Weber,^{h, 47} J. Weichert,²³ L. Welty-Rieger,⁵⁰ A. White,⁷⁵ D. Wicke,²⁵ M.R.J. Williams,⁴¹ G.W. Wilson,⁵⁵ M. Wobisch,⁵⁷ D.R. Wood,⁵⁹ T.R. Wyatt,⁴³ Y. Xie,⁴⁷ R. Yamada,⁴⁷ W.-C. Yang,⁴³ T. Yasuda,⁴⁷ Y.A. Yatsunencko,³⁴ W. Ye,⁶⁹ Z. Ye,⁴⁷ H. Yin,⁴⁷ K. Yip,⁷⁰ S.W. Youn,⁴⁷ T. Zhao,⁷⁹ B. Zhou,⁶⁰ J. Zhu,⁶⁰ M. Zielinski,⁶⁸ D. Zieminska,⁵¹ and L. Zivkovic⁷⁴

(The D0 Collaboration*)

¹Universidad de Buenos Aires, Buenos Aires, Argentina

²LAFEX, Centro Brasileiro de Pesquisas Físicas, Rio de Janeiro, Brazil

³Universidade do Estado do Rio de Janeiro, Rio de Janeiro, Brazil

⁴Universidade Federal do ABC, Santo André, Brazil

⁵Instituto de Física Teórica, Universidade Estadual Paulista, São Paulo, Brazil

⁶University of Science and Technology of China, Hefei, People's Republic of China

⁷Universidad de los Andes, Bogotá, Colombia

⁸Charles University, Faculty of Mathematics and Physics,

Center for Particle Physics, Prague, Czech Republic

⁹Czech Technical University in Prague, Prague, Czech Republic

¹⁰Center for Particle Physics, Institute of Physics,

Academy of Sciences of the Czech Republic, Prague, Czech Republic

¹¹Universidad San Francisco de Quito, Quito, Ecuador

¹²LPC, Université Blaise Pascal, CNRS/IN2P3, Clermont, France

¹³LPSC, Université Joseph Fourier Grenoble 1, CNRS/IN2P3,

Institut National Polytechnique de Grenoble, Grenoble, France

¹⁴CPPM, Aix-Marseille Université, CNRS/IN2P3, Marseille, France

¹⁵LAL, Université Paris-Sud, CNRS/IN2P3, Orsay, France

¹⁶LPNHE, Universités Paris VI and VII, CNRS/IN2P3, Paris, France

¹⁷CEA, Irfu, SPP, Saclay, France

¹⁸IPHC, Université de Strasbourg, CNRS/IN2P3, Strasbourg, France

¹⁹IPNL, Université Lyon 1, CNRS/IN2P3, Villeurbanne, France and Université de Lyon, Lyon, France

²⁰III. Physikalisches Institut A, RWTH Aachen University, Aachen, Germany

²¹Physikalisches Institut, Universität Freiburg, Freiburg, Germany

²²II. Physikalisches Institut, Georg-August-Universität Göttingen, Göttingen, Germany

²³Institut für Physik, Universität Mainz, Mainz, Germany

²⁴Ludwig-Maximilians-Universität München, München, Germany

²⁵Fachbereich Physik, Bergische Universität Wuppertal, Wuppertal, Germany

²⁶Panjab University, Chandigarh, India

²⁷Delhi University, Delhi, India

²⁸Tata Institute of Fundamental Research, Mumbai, India

²⁹University College Dublin, Dublin, Ireland

³⁰Korea Detector Laboratory, Korea University, Seoul, Korea

³¹CINVESTAV, Mexico City, Mexico

³²Nikhef, Science Park, Amsterdam, the Netherlands

³³Radboud University Nijmegen, Nijmegen, the Netherlands and Nikhef, Science Park, Amsterdam, the Netherlands

³⁴Joint Institute for Nuclear Research, Dubna, Russia

³⁵Institute for Theoretical and Experimental Physics, Moscow, Russia

³⁶Moscow State University, Moscow, Russia

³⁷Institute for High Energy Physics, Protvino, Russia

³⁸Petersburg Nuclear Physics Institute, St. Petersburg, Russia

³⁹Institució Catalana de Recerca i Estudis Avançats (ICREA) and Institut de Física d'Altes Energies (IFAE), Barcelona, Spain

⁴⁰Stockholm University, Stockholm and Uppsala University, Uppsala, Sweden

⁴¹Lancaster University, Lancaster LA1 4YB, United Kingdom

⁴²Imperial College London, London SW7 2AZ, United Kingdom

⁴³The University of Manchester, Manchester M13 9PL, United Kingdom

⁴⁴University of Arizona, Tucson, Arizona 85721, USA

⁴⁵University of California Riverside, Riverside, California 92521, USA

⁴⁶Florida State University, Tallahassee, Florida 32306, USA

⁴⁷Fermi National Accelerator Laboratory, Batavia, Illinois 60510, USA

⁴⁸University of Illinois at Chicago, Chicago, Illinois 60607, USA

- ⁴⁹Northern Illinois University, DeKalb, Illinois 60115, USA
⁵⁰Northwestern University, Evanston, Illinois 60208, USA
⁵¹Indiana University, Bloomington, Indiana 47405, USA
⁵²Purdue University Calumet, Hammond, Indiana 46323, USA
⁵³University of Notre Dame, Notre Dame, Indiana 46556, USA
⁵⁴Iowa State University, Ames, Iowa 50011, USA
⁵⁵University of Kansas, Lawrence, Kansas 66045, USA
⁵⁶Kansas State University, Manhattan, Kansas 66506, USA
⁵⁷Louisiana Tech University, Ruston, Louisiana 71272, USA
⁵⁸Boston University, Boston, Massachusetts 02215, USA
⁵⁹Northeastern University, Boston, Massachusetts 02115, USA
⁶⁰University of Michigan, Ann Arbor, Michigan 48109, USA
⁶¹Michigan State University, East Lansing, Michigan 48824, USA
⁶²University of Mississippi, University, Mississippi 38677, USA
⁶³University of Nebraska, Lincoln, Nebraska 68588, USA
⁶⁴Rutgers University, Piscataway, New Jersey 08855, USA
⁶⁵Princeton University, Princeton, New Jersey 08544, USA
⁶⁶State University of New York, Buffalo, New York 14260, USA
⁶⁷Columbia University, New York, New York 10027, USA
⁶⁸University of Rochester, Rochester, New York 14627, USA
⁶⁹State University of New York, Stony Brook, New York 11794, USA
⁷⁰Brookhaven National Laboratory, Upton, New York 11973, USA
⁷¹Langston University, Langston, Oklahoma 73050, USA
⁷²University of Oklahoma, Norman, Oklahoma 73019, USA
⁷³Oklahoma State University, Stillwater, Oklahoma 74078, USA
⁷⁴Brown University, Providence, Rhode Island 02912, USA
⁷⁵University of Texas, Arlington, Texas 76019, USA
⁷⁶Southern Methodist University, Dallas, Texas 75275, USA
⁷⁷Rice University, Houston, Texas 77005, USA
⁷⁸University of Virginia, Charlottesville, Virginia 22901, USA
⁷⁹University of Washington, Seattle, Washington 98195, USA
- (Dated: February 9, 2012)

We present a search for the pair production of scalar top quarks (\tilde{t}_1), the lightest supersymmetric partners of the top quarks, in $p\bar{p}$ collisions at a center-of-mass energy of 1.96 TeV, using data corresponding to an integrated luminosity of 7.3 fb^{-1} collected with the D0 experiment at the Fermilab Tevatron Collider. Each scalar top quark is assumed to decay into a b quark, a charged lepton, and a scalar neutrino ($\tilde{\nu}$). We investigate final states arising from $\tilde{t}_1\tilde{t}_1 \rightarrow b\bar{b}\mu\tau\tilde{\nu}\tilde{\nu}$ and $\tilde{t}_1\tilde{t}_1 \rightarrow b\bar{b}\tau\tau\tilde{\nu}\tilde{\nu}$. With no significant excess of events observed above the background expected from the standard model, we set exclusion limits on this production process in the $(m_{\tilde{t}_1}, m_{\tilde{\nu}})$ plane.

PACS numbers: 14.80.Ly, 12.60.Jv, 13.85.Rm

Supersymmetry (SUSY) [1] is a space-time symmetry that associates a bosonic partner with each standard model (SM) fermion, and a fermionic counterpart to each SM boson. The mass eigenstates of the scalar fermions, \tilde{f}_1 and \tilde{f}_2 , are the results of the mixing of the SUSY partners of the chiral states f_R and f_L . The mass splitting between \tilde{f}_1 and \tilde{f}_2 depends on the mass of the corresponding fermion. It has been suggested [2] that the large mass of the top quark (t) can induce a large splitting between the

two stop-mass eigenstates with the consequence that the lightest scalar top quark \tilde{t}_1 may be sufficiently light to be produced abundantly at the Fermilab Tevatron Collider. If R -parity [3] is conserved, scalar top quarks would be produced in pairs in $p\bar{p}$ collisions, either through gluon fusion or quark-antiquark annihilation.

In the minimal supersymmetric extension of the standard model (MSSM) [4] with R -parity conserved, squarks (\tilde{q}) usually decay directly into $\tilde{q} \rightarrow q \tilde{\chi}_1^0$ where the lightest neutralino $\tilde{\chi}_1^0$ is the lightest supersymmetric particle (LSP). At the Tevatron, this mode is kinematically disfavored for the lightest scalar top quark, because of the large mass of the top quark. If in addition, $m_{\tilde{t}_1} \leq m_b + m_{\tilde{\chi}_1^+}$, where $\tilde{\chi}_1^+$ is the lightest chargino, the decay channel $\tilde{t}_1 \rightarrow b\tilde{\chi}_1^+$ is not accessible, and the only two-body decay that would be allowed is the flavor changing decay $\tilde{t}_1 \rightarrow c\tilde{\chi}_1^0$ [5]. Searches related to this

*with visitors from ^aAugustana College, Sioux Falls, SD, USA, ^bThe University of Liverpool, Liverpool, UK, ^cUPIITA-IPN, Mexico City, Mexico, ^dSLAC, Menlo Park, CA, USA, ^eUniversity College London, London, UK, ^fCentro de Investigacion en Computacion - IPN, Mexico City, Mexico, ^gECFM, Universidad Autonoma de Sinaloa, Culiacán, Mexico, and ^hUniversität Bern, Bern, Switzerland. ⁱDESY, Hamburg, Germany, [‡]Deceased.

channel have been reported by the ALEPH, DELPHI, L3 and OPAL Collaborations [6]. The CDF [7] and D0 [8] Collaborations have searched for scalar top quarks in final states with acoplanar charm-jets and large imbalance in transverse momentum (\cancel{E}_T). Other possible decays are the three-body modes $\tilde{t}_1 \rightarrow bW\tilde{\chi}_1^0$, $\tilde{t}_1 \rightarrow bH^+\tilde{\chi}_1^0$, $\tilde{t}_1 \rightarrow b\ell\tilde{\nu}$, and $\tilde{t}_1 \rightarrow b\tilde{\ell}\nu$, where H^+ is the charged Higgs boson, and $\tilde{\nu}$ and $\tilde{\ell}$ are the sneutrinos and sleptons, superpartners of the neutrinos and leptons, respectively. A possible four-body decay, $\tilde{t}_1 \rightarrow b\tilde{\chi}_1^0 f\bar{f}'$, where f represents a fermion, mediated by virtual top quark, chargino, sbottom, slepton and first/second generation squark exchange, has also been suggested [9]. Searches related to this channel have been reported by the D0 Collaboration [10]. It is thought that the three-body decay modes may be important and even dominate the loop-induced $c\tilde{\chi}_1^0$ mode [11]. Searches for scalar top quark pair production in $b\bar{b}\ell\ell'\tilde{\nu}\tilde{\nu}$ final states have been reported by the ALEPH, L3, and OPAL Collaborations [6]. D0 [10, 12–15] and CDF [16] have searched for scalar top quark pairs in the final states $b\bar{b}\ell\ell'\tilde{\nu}\tilde{\nu}$, with leptons in $e\mu$, $\mu\mu$, or ee channels. No Tevatron searches have yet considered signatures with hadronically decaying τ leptons although SUSY could well appear at the Tevatron in final states with taus [17].

In this letter, we search for scalar top quark pair production in events with τ leptons, assuming that the branching fraction $B(\tilde{t}_1 \rightarrow b\ell\tilde{\nu}) = 1$ and that the sneutrino is either the LSP or decays invisibly. We search for stop pair production through the decay $\tilde{t}_1\tilde{t}_1 \rightarrow b\bar{b}\mu\tau\tilde{\nu}\tilde{\nu}$, or $\tilde{t}_1\tilde{t}_1 \rightarrow b\bar{b}\tau\tau(\rightarrow\mu\nu\nu)\tilde{\nu}\tilde{\nu}$, in a data sample corresponding to an integrated luminosity of 7.3 fb^{-1} at a center-of-mass energy of 1.96 TeV, collected with the D0 detector at the Fermilab Tevatron $p\bar{p}$ Collider between April 2002 and July 2010. The signal topology consists of one isolated muon, one isolated τ lepton, and \cancel{E}_T coming mainly from undetected sneutrinos, and unreconstructed or mis-measured jets.

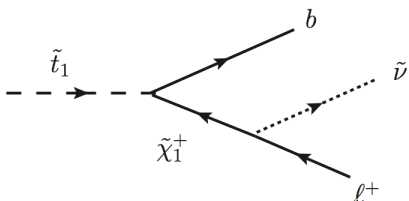


FIG. 1: Diagram contributing to the three-body decay $\tilde{t}_1 \rightarrow b\ell\tilde{\nu}$.

The three-body decay $\tilde{t}_1 \rightarrow b\ell\tilde{\nu}$ proceeds mainly through a virtual chargino $\tilde{\chi}_1^+$ (Fig. 1). In the MSSM, $\tilde{\chi}_1^+$ is the lightest mass eigenstate of the charged gaugino-higgsino mass matrix that is a mixing of the wino \tilde{W}^+ and the higgsino \tilde{H}^+ , SUSY partners of the W boson and the charged Higgs boson, respectively. If $\tilde{\chi}_1^+$ is wino-like, the leptonic decay $\tilde{\chi}_1^+ \rightarrow \ell^+\tilde{\nu}$ occurs with

equal rate to all lepton flavors. If $\tilde{\chi}_1^+$ is higgsino-like, the decay $\tilde{\chi}_1^+ \rightarrow \tau^+\tilde{\nu}$ is enhanced, owing to the large Yukawa coupling of the τ lepton. In that case, the decay $\tilde{t}_1 \rightarrow b\tau\tilde{\nu}$ can be dominant. We consider two scenarios in our search that depend on the composition of the chargino. The wino scenario is defined by $B(\tilde{t}_1 \rightarrow b\mu\tilde{\nu}) = B(\tilde{t}_1 \rightarrow b\tau\tilde{\nu}) = 1/3$. For the higgsino scenario, we choose $B(\tilde{t}_1 \rightarrow b\mu\tilde{\nu}) = 0.1$ and $B(\tilde{t}_1 \rightarrow b\tau\tilde{\nu}) = 0.8$, which correspond to the maximal values reached with a scan of the MSSM parameter space using SUSY-HIT [18]. In both scenarios, the signal is a combination of the $b\bar{b}\mu\tau\tilde{\nu}\tilde{\nu}$ and $b\bar{b}\tau\tau\tilde{\nu}\tilde{\nu}$ final states.

The D0 detector [19–21] is designed to optimize detection and identification of particles arising from $p\bar{p}$ interactions and comprises dedicated subsystems surrounding the interaction point. The central tracker resides within a liquid-argon/uranium sampling calorimeter and muon detectors. Charged particles are reconstructed using multi-layer silicon detectors and eight double layers of scintillating fibers in a 1.9 T magnetic field produced by a superconducting solenoid. After passing through the calorimeter, muons are identified using 1.9 T toroids and a muon system composed of three layers of drift tubes and scintillation counters. Events are selected for offline analysis through a three-level trigger system. All events contributing to this analysis are required to pass one of a suite of single-muon triggers based on information from the tracking and muon systems.

For each event, the best primary vertex (p_v) is selected from all the possible reconstructed interaction vertices as the one with smallest probability of originating from a minimum-bias interaction [22]. To ensure efficient reconstruction, the location of the primary vertex along the beam direction is restricted to $|z_{p_v}| < 60$ cm, where z_{p_v} is the longitudinal position with respect to the center of the detector.

Using central track segments pointing to hit patterns in the muon system, muons are identified in the region $|\eta| < 1.8$, where η is the pseudorapidity [23]. Their trajectories are required to have both drift-tube and scintillator hits that match a track in the central tracker. Muons that are not isolated are rejected if the sum of the transverse momenta of tracks inside a cone of radius $\mathcal{R} \equiv \sqrt{(\Delta\phi)^2 + (\Delta\eta)^2} = 0.5$ around each muon (ϕ being the azimuth), divided by the transverse momentum p_T^μ of the muon, is less than 0.15. The sum of the transverse energies in the calorimeter in an annulus of $0.1 < \mathcal{R} < 0.4$ around the muon, divided by p_T^μ , is also required to be less than 0.15. Only muons with $p_T^\mu \geq 15$ GeV are considered in the analysis. A veto on cosmic ray muons is applied using timing information from the muon system.

Decays of $\tau \rightarrow \text{hadrons} + \nu_\tau$ (called τ_h) are identified with a neural network [24] using as input variables (i) calorimeter clusters found with a cone algorithm of $\mathcal{R} = 0.3$, (ii) energy in an annular cone $0.3 \leq \mathcal{R} \leq 0.5$,

(iii) electromagnetic (EM) calorimeter subclusters, (iv) the multiplicity of tracks with $p_T > 1.5$ GeV within $\mathcal{R} < 0.5$ of the direction of the τ lepton, and (v) consistency of the invariant mass of the hadron system with that of τ decay. Three neural networks NN_τ are trained to identify tau decays corresponding to $\tau^\pm \rightarrow \pi^\pm \nu$ (τ_1), $\tau^\pm \rightarrow \pi^\pm \pi^0 \nu$ (τ_2), and $\tau^\pm \rightarrow \pi^\pm \pi^\pm \pi^\mp (\pi^0) \nu$ (τ_3). In addition, a selection on the output of NN_{el} , a neural network trained to separate τ_2 from electrons of similar signatures, is applied. The minimum transverse energy of the τ_h measured in the calorimeter, E_T^τ , is 12.5 GeV for τ_1 and τ_2 and 15 GeV for τ_3 . The sum of the transverse momenta of the τ -associated tracks, p_T^{trk} , is required to exceed 7, 5, and 10 GeV, for τ_1 , τ_2 , and τ_3 , respectively. In addition, at least one track with $p_T > 7$ GeV is required for τ_3 . Finally, only candidates with $|\eta_{\tau_h}| < 1$ and $p_T^{\text{trk}}/E_T^\tau > (0.65, 0.5, 0.5)$ for (τ_1, τ_2, τ_3) are selected.

Jets are reconstructed from energies deposited in calorimeter towers using an iterative midpoint cone algorithm [25], with a cone radius $\mathcal{R} = 0.5$. Jet energies are calibrated to the particle-level jets using correction factors derived primarily from the transverse momentum balance in photon plus jets events [26]. Only jets with $p_T^{\text{jet}} > 15$ GeV and $|\eta| < 2.5$ are considered in this analysis and jets in the vicinity of a τ_h candidate ($\mathcal{R} < 0.5$) are discarded.

The \cancel{E}_T is calculated from the calorimeter energy, corrected for jet, EM, and τ energy scales and for the transverse momentum of selected muons.

Monte Carlo (MC) events for signal are simulated using MADGRAPH/MADEVENT [27] and PYTHIA [28] for parton-level generation and hadronization, respectively. We consider a range of scalar top quark mass values from 100 to 200 GeV, generated in steps of 20 GeV. The range of probed sneutrino masses extends from 40 to 140 GeV in steps of 20 GeV. For each hypothesis, the MSSM parameters are estimated from SUSPECT [29] and SDECAY [30]. The next-to-leading order (NLO) scalar top quark pair production cross section is calculated with PROSPINO 2.0 [31], using CTEQ6.1M parton distribution functions (PDF) [32, 33]. The calculations are performed with the renormalization and factorization scales $\mu_{r,f}$ equal to the scalar top quark mass $m_{\tilde{t}_1}$, $\frac{1}{2} m_{\tilde{t}_1}$, and $2 m_{\tilde{t}_1}$ to estimate uncertainty on the nominal value through the impact of the two excursions. These uncertainties are combined quadratically with uncertainties on the PDF [32, 33] to provide a total theoretical uncertainty of 18% to 20% on the scalar top quark cross section.

The kinematics for signal are determined both by $m_{\tilde{t}_1}$ and by the mass difference $\Delta m = m_{\tilde{t}_1} - m_{\tilde{\nu}}$. The p_T of the leptons and b quarks decrease on average for smaller values of Δm , and \cancel{E}_T is correlated with both $m_{\tilde{t}_1}$ and Δm . We choose two signal points $[m_{\tilde{t}_1}, m_{\tilde{\nu}}] = (180, 60)$ GeV and $(120, 80)$ GeV, labeled “Signal A” and “Signal B” in the following, to illustrate the impact of the selection criteria for large $m_{\tilde{t}_1}$ and Δm (Signal A)

and for low $m_{\tilde{t}_1}$ and Δm (Signal B).

The dominant SM backgrounds to the pair production of scalar top quarks are from $Z/\gamma^*(\rightarrow \tau^+\tau^-)+\text{jets}$; $Z/\gamma^*(\rightarrow \mu^+\mu^-)+\text{jets}$; diboson production (WW, WZ, ZZ); $t\bar{t}$; $W+\text{jets}$, and instrumental background from multijet (MJ) processes. All but the latter are estimated through MC simulations. Vector boson pair production is simulated with PYTHIA, while the other backgrounds are simulated at the parton level using ALPGEN [34] and PYTHIA for hadronization and parton showering.

Correction factors for MC estimated from data are applied to lessen the impact of minor mismodeling of detector response. These corrections are related to the instantaneous luminosity, the position of the beam spot, identification efficiencies for μ and τ , vector boson p_T , and jet, muon, and τ_h energy resolutions.

The instrumental background originates either from incorrectly-identified, isolated muons (arising for example from semi-leptonic b decays) or from misidentified τ_h (jets mimicking τ_h signatures). This is estimated by changing the requirements on muon isolation and on the τ_h NN_τ outputs for each type of tau after the subtraction of the MC contributions corresponding to non-instrumental background. Normalization factors for these samples are estimated assuming that MJ processes have equal amounts of like-charge and opposite-charge $\mu\tau$ events.

The search of scalar top quark pairs proceeds in three steps: two event selections, labeled “Selection-1” and “Selection-2” below, and then a multivariate analysis.

Selection-1 requires candidates to contain exactly one muon and τ_h of opposite electric charge, and to have a minimum separation of $\mathcal{R}(\mu, \tau_h) > 0.5$ between the two leptons. No specific requirement on jets is applied at this stage, but events having a jet in the vicinity of the muon ($\Delta\mathcal{R} < 0.5$) are rejected. Events with low values of the azimuthal angle difference between the leptons and \cancel{E}_T , which are often due to issues with lepton reconstruction, are removed by requiring $\Delta\phi(\mu, \cancel{E}_T) > 0.5$ and $\Delta\phi(\tau_h, \cancel{E}_T) > 0.5$. At this stage of the analysis, 3387 data events remain while 3453 ± 29 (stat) ± 440 (syst) events are expected from background. The main background is from $Z/\gamma^*(\rightarrow \tau^+\tau^-)+\text{jets}$, $W+\text{jets}$, and MJ events, as can be seen in Table I. Signal efficiencies do not exceed 4% for large Δm , and are lower than 0.1% for $\Delta m < 20$ GeV.

Jets in scalar top quark pair events originate mainly from the hadronization of b quarks, whereas in $Z/\gamma^*(\rightarrow \tau^+\tau^-)+\text{jets}$ and $W+\text{jets}$ backgrounds jets correspond predominantly to initial-state gluon radiation that provides a lower jet multiplicity. To maintain sensitivity to low Δm signals, while rejecting a substantial part of the background, at least one jet is required in each event, which corresponds to Selection-2. Fig. 2 shows the jet multiplicity for the different τ_h decays. After this selection, 893 events remain, while a total background of

TABLE I: Numbers of events observed and expected from SM background processes and the two signal samples A and B at the Selection-1 stage for τ_h (τ_1 , τ_2 , τ_3) and their sum. The uncertainties quoted in the Table are statistical.

| Process | τ_1 | τ_2 | τ_3 | all τ |
|---|-----------------|-------------------|-------------------|-------------------|
| $Z/\gamma^*(\rightarrow\tau^+\tau^-)+\text{jets}$ | 162.6 | 994.4 | 352.3 | 1509.4 |
| $Z/\gamma^*(\rightarrow\mu^+\mu^-)+\text{jets}$ | 38.7 | 91.6 | 48.3 | 178.6 |
| diboson | 7.5 | 40.5 | 16.9 | 65.0 |
| $t\bar{t}$ | 3.2 | 27.3 | 10.7 | 41.3 |
| $W+\text{jets}$ | 125.1 | 631.1 | 421.1 | 1177.2 |
| Instrumental | 54.7 | 233.1 | 193.4 | 481.3 |
| Background total | 392.0 ± 6.0 | 2018.1 ± 16.9 | 1042.8 ± 12.6 | 3452.8 ± 28.6 |
| Data | 388 | 1937 | 1062 | 3387 |
| Wino scenario | | | | |
| Signal A | 2.3 ± 0.3 | 17.4 ± 0.8 | 4.7 ± 0.4 | 24.4 ± 1.0 |
| Signal B | 4.4 ± 1.3 | 21.4 ± 3.0 | 7.1 ± 1.7 | 32.9 ± 3.7 |
| Higgsino scenario | | | | |
| Signal A | 2.9 ± 0.3 | 20.5 ± 0.9 | 5.3 ± 0.5 | 28.6 ± 1.1 |
| Signal B | 3.8 ± 1.2 | 20.5 ± 2.9 | 6.9 ± 1.6 | 31.1 ± 3.6 |

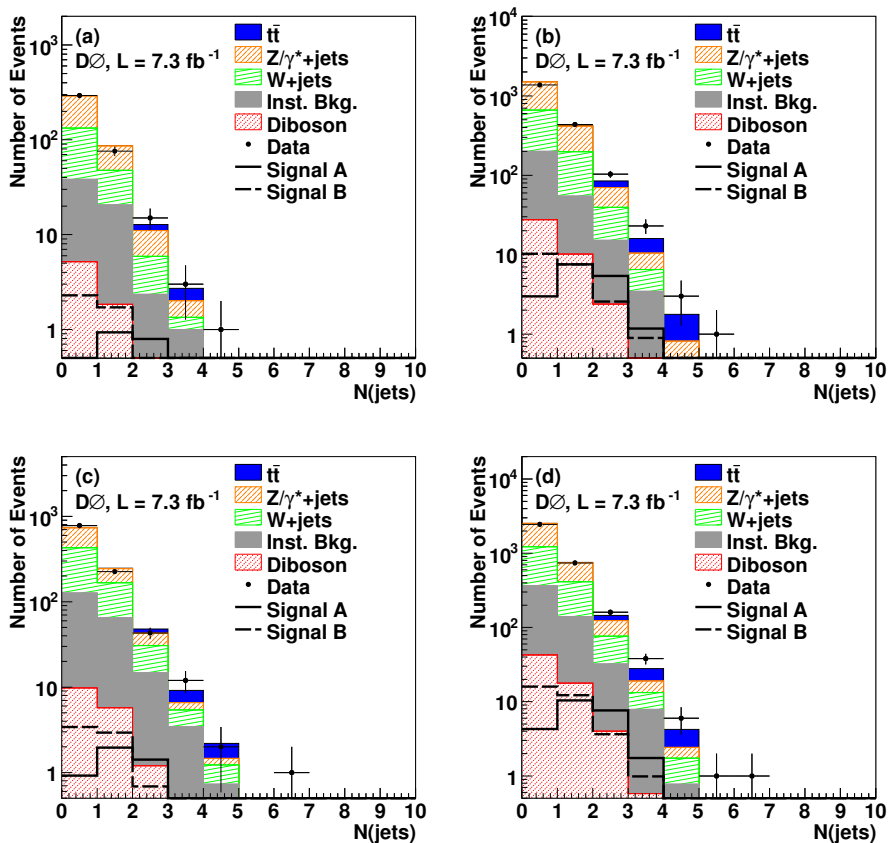


FIG. 2: (Color online) Distributions of the number of jets after the preselection for (a) τ type 1, (b) τ type 2, (c) τ type 3, and (d) their event sum. Signal A and Signal B correspond to the wino scenario.

905 ± 10 (stat) ± 127 (syst) events is expected (see Table II).

The separation of scalar top quark signal and background is improved through an implementation of Boosted Decision Trees (BDT) [35]. A decision tree classifies events on the basis of cumulative selection criteria

that define disjoint subsets of events, each with a different signal purity. The decision tree is redefined iteratively by creating subsets of events called nodes. Each node is split into two subsets on the basis of the strongest discriminant for that sample. An impurity measure i is estimated for each node from the

TABLE II: Numbers of events observed and expected from SM background processes and for the two signal samples A and B, after the final selection on $N(\text{jets}) > 0$. The quoted uncertainties correspond to statistical sources.

| Process | τ_1 | τ_2 | τ_3 | all τ | $N(\text{jets}) = 1$ | $N(\text{jets}) = 2$ | $N(\text{jets}) > 2$ |
|--|----------------|-----------------|-----------------|-----------------|----------------------|----------------------|----------------------|
| $Z/\gamma^*(\rightarrow \tau^+\tau^-)+\text{jets}$ | 35.6 | 226.2 | 79.5 | 341.3 | 301.6 | 34.6 | 5.0 |
| $Z/\gamma^*(\rightarrow \mu^+\mu^-)+\text{jets}$ | 8.0 | 20.7 | 10.4 | 39.1 | 33.5 | 4.7 | 0.9 |
| diboson | 2.3 | 12.5 | 6.9 | 21.7 | 17.7 | 3.3 | 0.7 |
| $t\bar{t}$ | 3.0 | 25.6 | 10.1 | 38.7 | 8.1 | 20.0 | 10.6 |
| $W+\text{jets}$ | 30.4 | 166.5 | 117.5 | 314.4 | 301.6 | 36.7 | 6.0 |
| Instrumental | 20.6 | 55.0 | 74.1 | 149.8 | 122.4 | 20.1 | 7.3 |
| Background total | 99.9 ± 2.3 | 506.6 ± 5.4 | 298.5 ± 4.9 | 905.1 ± 9.6 | 755.1 ± 8.4 | 119.4 ± 2.0 | 30.6 ± 0.8 |
| Data | 90 | 532 | 271 | 893 | 738 | 116 | 39 |
| Wino scenario | | | | | | | |
| Signal A | 1.9 ± 0.3 | 13.9 ± 0.7 | 3.7 ± 0.4 | 19.5 ± 0.9 | 10.4 ± 0.6 | 7.1 ± 0.5 | 2.0 ± 0.3 |
| Signal B | 2.0 ± 0.9 | 10.6 ± 2.1 | 3.6 ± 1.2 | 16.3 ± 2.6 | 12.2 ± 2.3 | 3.1 ± 1.1 | 1.0 ± 0.6 |
| Higgsino scenario | | | | | | | |
| Signal A | 2.3 ± 0.3 | 16.2 ± 0.8 | 4.2 ± 0.4 | 22.7 ± 1.0 | 11.8 ± 0.7 | 8.6 ± 0.6 | 2.3 ± 0.3 |
| Signal B | 1.8 ± 0.8 | 9.9 ± 2.0 | 3.1 ± 1.1 | 14.8 ± 2.4 | 10.9 ± 2.0 | 2.9 ± 1.0 | 1.0 ± 0.6 |

weighted number of signal S and background B events in the node. For a given split, the decrease of impurity $\Delta i = i(S, B) - i(S_L, B_L) - i(S_R, B_R)$, where L and R stand for left and right daughter nodes, is calculated. The best splitting gives the largest Δi . We use the Gini index [35] defined as $SB/(S+B)^2$ as a measure of impurity. Terminal nodes are called leaves. Each leaf has a purity value defined by $S/(S+B)$. One of the main advantage of decision trees over analyses using simple requirements is that events that fail any individual selection criteria continue to be considered by the algorithm.

The performance of the decision tree is improved by the boosting technique [36]. The basic principle is to create a tree, calculate an associated uncertainty, and create a new tree with a smaller uncertainty by re-weighting the misclassified events. We use adaptative boosting, known in the literature as AdaBoost [36]. The associated uncertainty ϵ_n of a tree indexed by n is estimated as the fraction of misclassified events. The boosting weight of the n^{th} tree is $\alpha_n = \beta \ln((1 - \epsilon_n)/\epsilon_n)$ where β is an empirically determined parameter called boosting parameter. Misclassified events are given an additional multiplicative weight of e^{α_n} and the resulting new tree indexed by $n+1$ is used to retrain the BDT and reduce the number of misclassified events. This procedure is repeated N times, where N is the number of boosting cycles. For the scalar top quark search, the best signal to background separation occurs for $\beta = 0.5$ and $N = 40$.

To optimize the sensitivity of the analysis, three sub-samples are selected according to the jet multiplicity per event: $N(\text{jets})=1$, $N(\text{jets})=2$, $N(\text{jets})>2$. Since there are many SUSY mass points, and their characteristics differ significantly, the generated BDTs are trained and tested for each sample and each SUSY point using the implementation of the TMVA [37] library. The five most sensitive input variables for the BDTs trained with samples of Signal A and Signal B are given in Table III. To minimize bias, samples are split into three parts: 1/3 for

training, 1/3 for testing and 1/3 for analysis. The distributions of the BDT outputs trained with Signals A and B are shown in Figs. 3 and 4 for the wino and higgsino scenarios, respectively.

The predicted numbers of background and signal events depend on measurements and parametrizations that have non-negligible systematic uncertainties, which can either affect exclusively the normalizations of backgrounds or the signal efficiency, or modify also the differential distribution of the BDT discriminant. The main sources involve muon identification and reconstruction efficiencies (2%), τ_h identification and reconstruction (10%, 4%, and 5% for τ_1 , τ_2 and τ_3 , respectively), trigger (5%), luminosity (6.1%) [38], jet energy calibration (3.2% for the background, 1.5% to 2.6% for signal), jet identification efficiency and energy resolution (5% for the background, 1% to 6% for signal). Systematic uncertainties related to reconstructed objects are estimated by changing each quantity by one standard deviation (s.d), and gauging the impact on the final measurement. Additional uncertainties arise from the choice of PDF, which affects the cross sections for the background components (6.3% for $Z/\gamma^*(\rightarrow \tau^+\tau^-)+\text{jets}$ and $Z/\gamma^*(\rightarrow \mu^+\mu^-)+\text{jets}$, 15% for $W+\text{jets}$ and 10% for $t\bar{t}$; 5.6%, 8.1%, and 5.5% for WW , WZ , and ZZ , respectively) and for signal (18% to 20%). To estimate the systematic uncertainties related to instrumental background, a MC scalar top quark signal is added as a background contribution during the stages that consider distribution and normalization of the MJ background. Each scalar top quark signal is considered, and the largest relative changes in the distribution and the normalization of the instrumental background are thereby estimated. The resulting uncertainties correspond to 5% and 10% for the normalization and the functional dependence, respectively.

There is no significant excess of events observed above the predicted background, and we therefore combine the numbers of expected signal and background events, with

TABLE III: Listing of the five most sensitive input variables used for each BDT training and testing. The significance of \cancel{E}_T , $\text{Sig}(\cancel{E}_T)$, is defined as the likelihood that the \cancel{E}_T in an event is consistent with a fluctuation of the resolution on the p_T measurements on the selected leptons and jets. S_T is the sum of the lepton p_T and of the \cancel{E}_T . The transverse mass M_T is defined as $M_T(A, B) = \sqrt{2p_T^A p_T^B (1 - \cos \Delta\phi(A, B))}$. H_T is equal to the scalar sum of the E_T of the jets.

| | Wino scenario | | | Higgsino scenario | | |
|----------|---|--|--|---|--|--|
| | $N(\text{jets})=1$ | $N(\text{jets})=2$ | $N(\text{jets})\geq 3$ | $N(\text{jets})=1$ | $N(\text{jets})=2$ | $N(\text{jets})\geq 3$ |
| Signal A | S_T | $\Delta\phi^{\min}(\text{jet}, \cancel{E}_T)$ | $\Delta\phi^{\min}(\text{jet}, \cancel{E}_T)$ | $\Delta\phi^{\min}(\text{jet}, \cancel{E}_T)$ | $\text{Mass}(\mu, \tau)$ | $\Delta\phi^{\min}(\text{jet}, \cancel{E}_T)$ |
| | $\eta(\text{leading jet})$ | $\eta(\text{leading jet})$ | $\text{Sig}(\cancel{E}_T)$ | $\eta(\text{leading jet})$ | $\eta(\text{leading jet})$ | H_T |
| | $\Delta\mathcal{R}^{\max}(\mu, \text{jet})$ | $\Delta\mathcal{R}^{\max}(\tau, \text{jet})$ | $\Delta\mathcal{R}^{\max}(\tau, \text{jet})$ | $\Delta\mathcal{R}^{\max}(\tau, \text{jet})$ | $\Delta\mathcal{R}^{\max}(\mu, \text{jet})$ | $\Delta\mathcal{R}^{\max}(\tau, \text{jet})$ |
| | $M_T(\mu, \cancel{E}_T)$ | $\Delta\phi(\mu\tau, \cancel{E}_T)$ | E_T^{τ} | $\text{Sig}(\cancel{E}_T)$ | $\Delta\phi(\mu + \tau, \cancel{E}_T)$ | $\text{Mass}(\mu, \tau)$ |
| | $\text{Mass}(\text{lept}, \text{jet})$ | $\Delta\mathcal{R}^{\max}(\mu, \text{jet})$ | $p_T(\text{leading jet})$ | $\text{Mass}(\text{lept}, \text{jet})$ | $M_T(\tau, \cancel{E}_T)$ | $\text{Mass}(\mu, \text{jet})$ |
| Signal B | $\text{Sig}(\cancel{E}_T)$ | $\Delta\phi^{\min}(\text{jet}, \cancel{E}_T)$ | $\Delta\phi^{\min}(\text{jet}, \cancel{E}_T)$ | $\Delta\eta(\mu, \tau)$ | $\Delta\phi^{\min}(\text{jet}, \cancel{E}_T)$ | $\Delta\phi(\mu, \tau)$ |
| | $\eta(\tau)$ | $\eta(\text{leading jet})$ | $\text{Sig}(\cancel{E}_T)$ | S_T | $\eta(\text{leading jet})$ | $\Delta\phi(\text{leading jet}, \cancel{E}_T)$ |
| | S_T | $\Delta\mathcal{R}^{\min}(\tau, \text{jet})$ | $\Delta\phi(\mu + \tau, \cancel{E}_T)$ | $\eta(\tau)$ | $\Delta\mathcal{R}^{\min}(\tau, \text{jet})$ | $\Delta\mathcal{R}^{\max}(\tau, \text{jet})$ |
| | $\Delta\phi(\mu, \tau)$ | $\Delta\phi(\text{next-to-leading jet}, \cancel{E}_T)$ | $\Delta\phi(\text{leading jet}, \cancel{E}_T)$ | $\Delta\phi(\mu, \tau)$ | $\Delta\phi(\text{leading jet}, \cancel{E}_T)$ | $\Delta\phi(\mu, \cancel{E}_T)$ |
| | $\text{Mass}(\text{lept}, \text{jet})$ | $\Delta\mathcal{R}^{\min}(\mu, \text{jet})$ | $\text{Mass}(\mu, \text{jet})$ | $\text{Mass}(\text{lept}, \text{jet})$ | $\Delta\phi(\mu + \tau, \cancel{E}_T)$ | $\Delta\phi(\tau, \cancel{E}_T)$ |

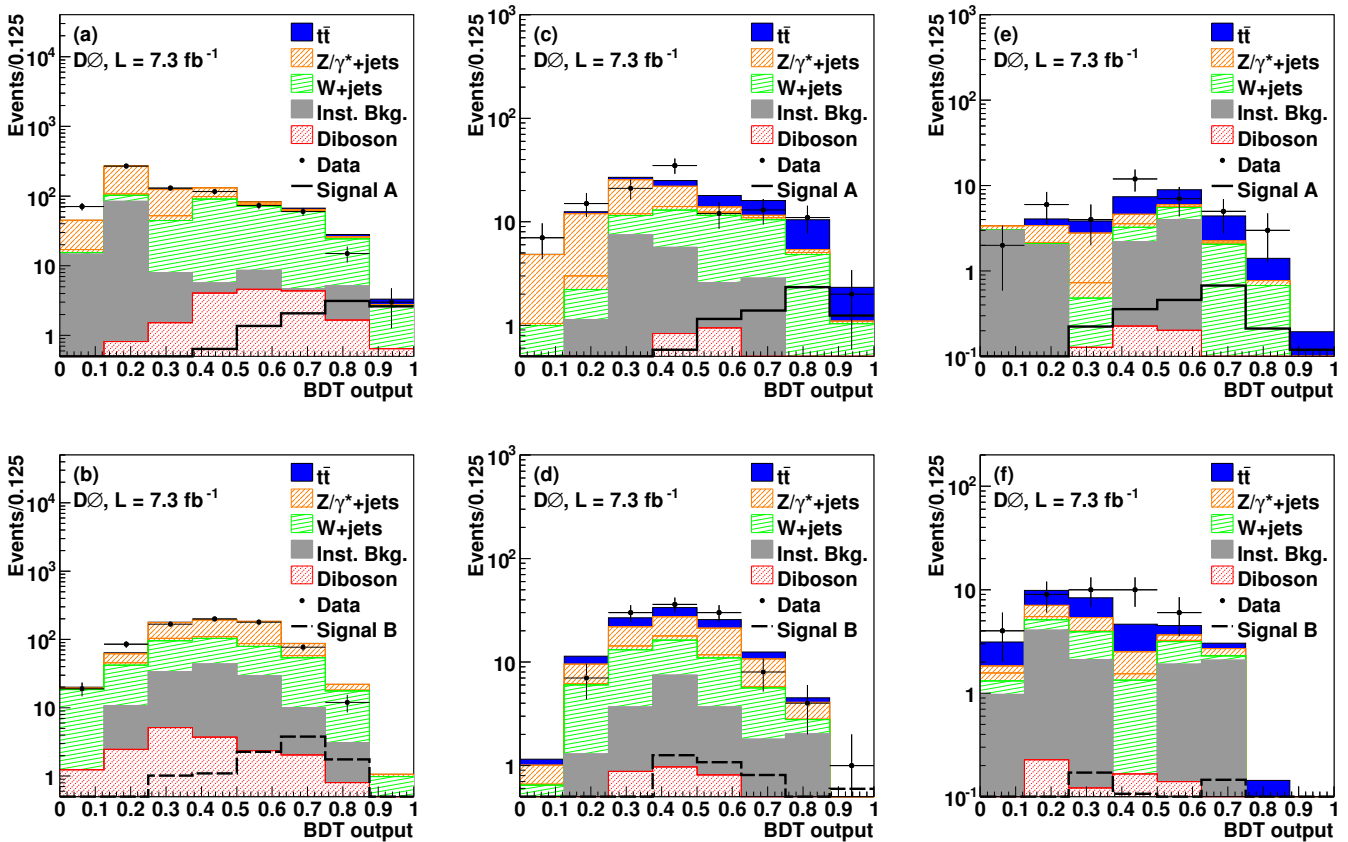


FIG. 3: (Color online) Distributions of the BDT output discriminants, in the wino scenario, for the sample with $N(\text{jets})=1$, (a) for Signal A, (b) for Signal B; $N(\text{jets})=2$, (c) for Signal A, (d) for Signal B; $N(\text{jets})> 2$, (e) for Signal A, (f) for Signal B.

their corresponding uncertainties, and the numbers of events observed in data obtained from the BDT outputs for each SUSY point, to calculate upper limits on the cross sections for signal at the 95% CL using the modified frequentist approach [39]. The bins of the BDT outputs corresponding to $N(\text{jets})=1, 2$, and > 2 , are treated as separate channels, and their likelihoods are combined

taking into account the correlations of both systematic uncertainties affecting exclusively the normalization of backgrounds and signal efficiencies and also of those that change the distribution of the BDT discriminant. The limits are calculated using the confidence level $CL_S = CL_{S+B}/CL_B$ where CL_{S+B} and CL_B are the confidence levels for the signal+background and background-only

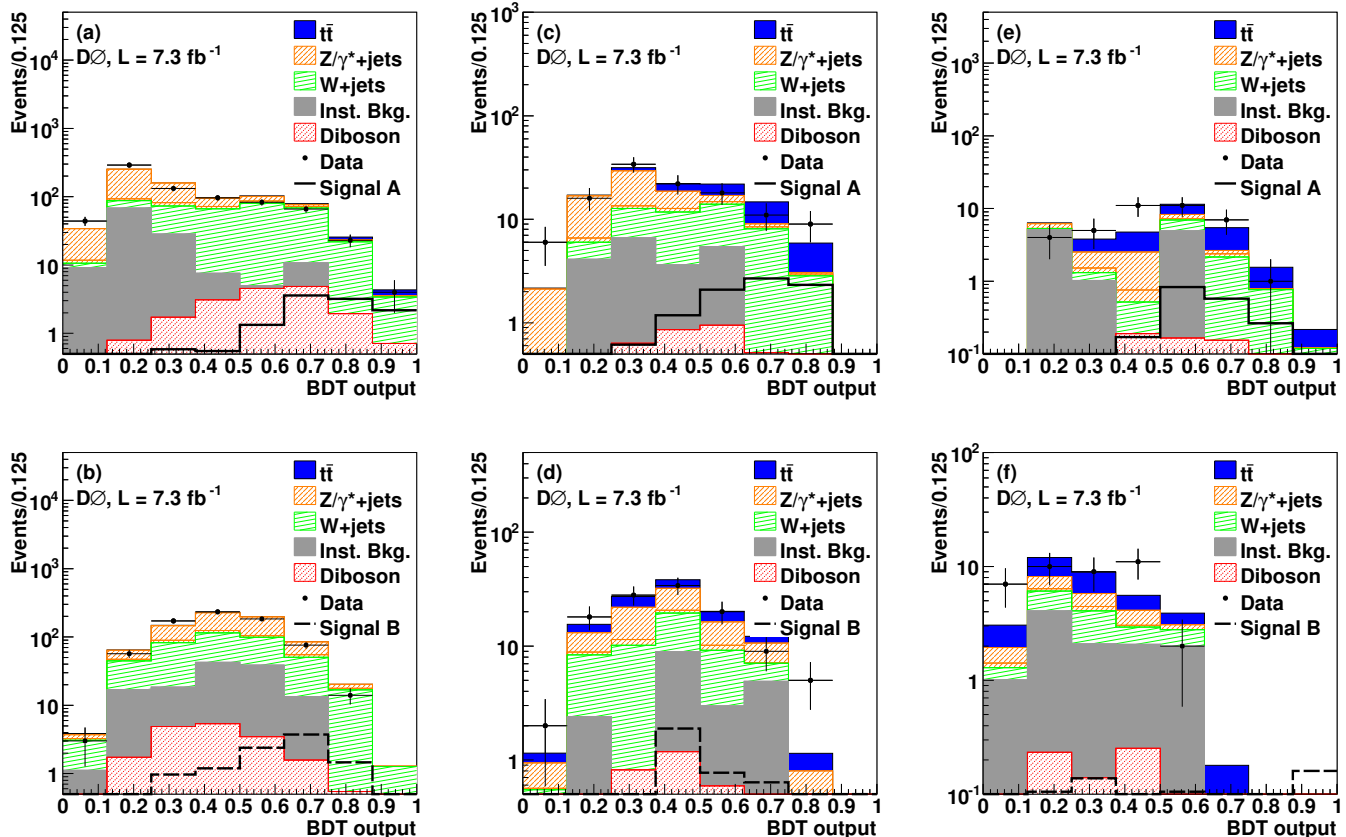


FIG. 4: (Color online) Distributions of the BDT output discriminants, in the higgsino scenario, for the sample with $N(\text{jets})=1$, (a) for Signal A, (b) for Signal B; $N(\text{jets})=2$, (c) for Signal A, (d) for Signal B; $N(\text{jets})>2$, (e) for Signal A, (f) for Signal B.

hypotheses, respectively [39]. Exclusion regions are given on Figs. 5 and 6 as a function of the scalar top quark and sneutrino masses. These results are obtained under the assumption $B(\tilde{t}_1 \rightarrow b\mu\tilde{\nu}) = B(\tilde{t}_1 \rightarrow b\tau\tilde{\nu}) = 1/3$ (Fig. 5, wino scenario) and $B(\tilde{t}_1 \rightarrow b\mu\tilde{\nu}) = 0.1$, $B(\tilde{t}_1 \rightarrow b\tau\tilde{\nu}) = 0.8$ (Fig. 6, higgsino scenario). For larger mass differences between the scalar top quark and the sneutrino, a scalar top quark mass lower than 200 GeV is excluded. The search is sensitive to a possible signal in the mass region up to $\Delta m = 60$ GeV for $m_{\tilde{t}_1} = 140$ GeV, with the observed limit being within one standard deviation of the expected limit.

In summary, a search for scalar top quark pair production in $p\bar{p}$ collisions at $\sqrt{s} = 1.96$ TeV has been performed in a dataset corresponding to an integrated luminosity of 7.3 fb^{-1} . Events containing one muon, one τ decaying hadronically, at least one jet, and missing transverse energy have been considered in this analysis. No evidence is found for the production of the lightest scalar top quark, and 95% CL exclusion limits are set in the plane $[m_{\tilde{t}_1}, m_{\tilde{\nu}}]$. The largest scalar top quark mass excluded is 200 GeV for a sneutrino mass of 45 GeV, and the largest sneutrino mass excluded is 85 GeV for a

scalar top quark mass of 160 GeV. This is the first Tevatron limit obtained from a study of final states containing τ leptons from $\tilde{t}_1\tilde{t}_1 \rightarrow b\bar{b}\mu\tau E_T$.

We thank the staffs at Fermilab and collaborating institutions, and acknowledge support from the DOE and NSF (USA); CEA and CNRS/IN2P3 (France); FASI, Rosatom and RFBR (Russia); CNPq, FAPERJ, FAPESP and FUNDUNESP (Brazil); DAE and DST (India); Colciencias (Colombia); CONACyT (Mexico); NRF (Korea); CONICET and UBACyT (Argentina); FOM (The Netherlands); STFC and the Royal Society (United Kingdom); MSMT and GACR (Czech Republic); BMBF and DFG (Germany); SFI (Ireland); The Swedish Research Council (Sweden); and CAS and CNSF (China).

-
- [1] See, for example: P. Fayer, S. Ferrara, Phys. Rep. **32**, 249 (1977).
 - [2] J. Ellis and S. Rudaz, Phys. Lett. B **128**, 248 (1983).
 - [3] See, for example: R. Barbier *et al.*, Phys. Rep. **420**, 1 (2005).
 - [4] S. Dimopoulos, Nucl. Phys. **B 193**, 150 (1981).

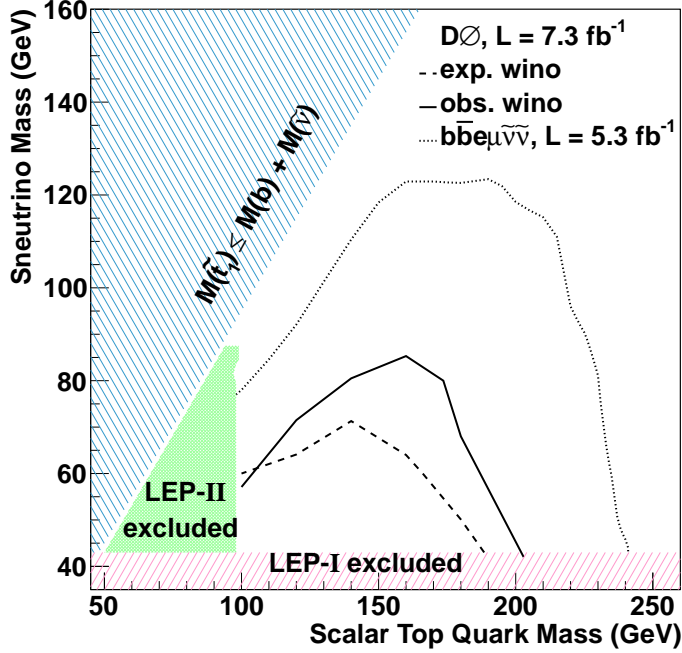


FIG. 5: (Color online) The 95% CL contour of exclusion in the sneutrino versus scalar top quark mass plane obtained for the assumption $B(\tilde{t}_1 \rightarrow b\mu\tilde{\nu}) = B(\tilde{t}_1 \rightarrow b\tau\tilde{\nu}) = 1/3$ (wino scenario). Shaded areas represent the kinematically forbidden region and the LEP-I [40] and LEP-II [6] exclusions. The dashed and continuous lines represent, respectively, the expected and observed 95% CL exclusion limits for this analysis. The region excluded by a recent D0 search [15] in the $\tilde{t}_1\tilde{t}_1 \rightarrow b\bar{b}e\mu\tilde{\nu}\tilde{\nu}$ final state in the wino scenario is indicated by the dotted line.

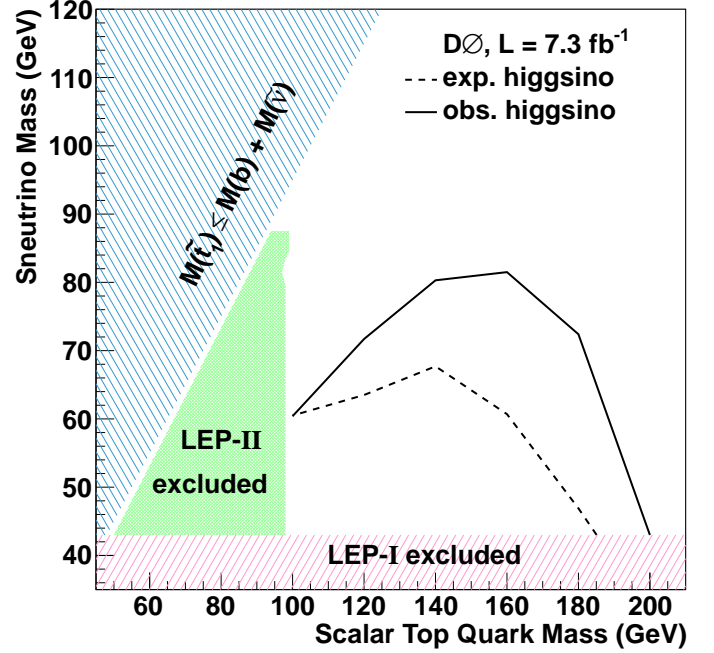


FIG. 6: (Color online) The 95% CL contour of exclusion in the sneutrino versus scalar top quark mass plane obtained for the assumption $B(\tilde{t}_1 \rightarrow b\mu\tilde{\nu}) = 0.1$ and $B(\tilde{t}_1 \rightarrow b\tau\tilde{\nu}) = 0.8$ (higgsino scenario). Shaded areas represent the kinematically forbidden region and the LEP-I [40] and LEP-II [6] exclusions. The dashed and continuous lines represent, respectively, the expected and observed 95% CL exclusion limits for this analysis.

- [5] K.I. Hikasa and M. Kobayashi, Phys. Rev. D **36**, 724 (1987).
- [6] LEP SUSY Working Group (ALEPH, DELPHI, L3, and OPAL Collaborations), LEPSUSYWG/01-02.1 (2001), URL <http://lepsusy.web.cern.ch/lepsusy/>.
- [7] T. Aaltonen *et al.* (CDF Collaboration), Phys. Rev. D **79**, 072010 (2007).
- [8] V.M. Abazov *et al.* (D0 Collaboration), Phys. Lett. B **665**, 1 (2008).
- [9] C. Boehm, A. Djouadi, and Y. Mambrini, Phys. Rev. D **61**, 095006 (2000).
- [10] V.M. Abazov *et al.* (D0 Collaboration), Phys. Lett. B **581**, 147 (2004).
- [11] A. Djouadi and Y. Mambrini, Phys. Rev. D **63**, 115005 (2001).
- [12] V.M. Abazov *et al.* (D0 Collaboration), Phys. Rev. Lett. **88**, 171802 (2002).
- [13] V.M. Abazov *et al.* (D0 Collaboration), Phys. Lett. B **659**, 500 (2008).
- [14] V.M. Abazov *et al.* (D0 Collaboration), Phys. Lett. B **675**, 289 (2009).
- [15] V.M. Abazov *et al.* (D0 Collaboration), Phys. Lett. B **696**, 321 (2011).
- [16] T. Aaltonen *et al.* (CDF Collaboration), Phys. Rev. D **82**, 092001 (2010).
- [17] V. Barger *et al.*, in *Report of SUGRA Working Group for Run II of the Tevatron*, edited by T. Falk and X. Tata, Fermilab-Pub-00-386-T (2000).
- [18] A. Djouadi, M.M. Muhlleitner, M. Spira, Acta Phys. Polon. B **38**, 635 (2007).
- [19] V.M. Abazov *et al.* (D0 Collaboration), Nucl. Instrum. Meth. Phys. Res. A **565**, 463 (2006).
- [20] M. Abolins *et al.*, Nucl. Instrum. Meth. Phys. Res. A **584**, 75 (2008).
- [21] R. Angstadt *et al.*, Nucl. Instrum. Meth. Phys. Res. A **622**, 298 (2010).
- [22] V.M. Abazov *et al.* (D0 Collaboration), Phys. Rev. D **74**, 112004 (2006).
- [23] The pseudorapidity is defined as $\eta = -\ln[\tan(\theta/2)]$, with θ being the polar angle with respect to the proton beam direction, relative to the center of the detector.
- [24] V.M. Abazov *et al.* (D0 Collaboration), Phys. Lett. B **670**, 292 (2009).
- [25] G.C. Blazey *et al.*, in *Proceedings of the Workshop: QCD and Weak Boson Physics in Run II*, edited by U. Baur, R.K. Ellis, and D. Zeppenfeld, Fermilab-Pub-00/297 (2000).
- [26] V.M. Abazov *et al.* (D0 Collaboration), arXiv:1110.3771 [hep-ex], Fermilab-PUB-11/547-E, submitted to Phys. Rev. D.

- [27] J. Alwall *et al.*, *J. High Energy Phys.* **709**, 028 (2007).
- [28] T. Sjöstrand *et al.*, *Comput. Phys. Commun.* **135**, 238 (2001).
- [29] A. Djouadi, J-L. Kneur, and G. Moultaka, *Comput. Phys. Comm.* **176**, 426 (2007).
- [30] M. Mühlleitner, *Acta Phys. Polon. B* **35**, 2753 (2004).
- [31] W. Beenakker, R. Höpker, and M. Spira, arXiv:hep-ph/9611232 (1996).
- [32] J. Pumplin *et al.*, *J. High Energy Phys.* **07**, 012 (2002).
- [33] D. Stump *et al.*, *J. High Energy Phys.* **10**, 046 (2003).
- [34] M. Mangano *et al.*, *J. High Energy Phys.* **07**, 001 (2003).
- [35] L. Breiman *et al.*, “Classification and Regression Trees”, Wadsworth (1984).
- [36] Y. Freund and R. E. Schapire, in *Machine Learning: Proceedings of the Thirteenth International Conference*, edited by L. Saitta (Morgan Kaufmann, San Francisco, 1996), 148.
- [37] BDTs have been computed with the Toolkit for Multivariate Data Analysis (TMVA) package (<http://tmva.sourceforge.net/>) implemented in ROOT (<http://root.cern.ch>) v5.27.
- [38] T. Andeen *et al.*, FERMILAB-TM-2365 (2007).
- [39] T. Junk, *Nucl. Instrum. Meth. Phys. Res. A* **434**, 435 (1999).
- [40] K. Nakamura *et al.* (Particle Data Group), *J. Phys. G* **37**, 1 (2010).